Wave packet and quasiclassical trajectory calculations for the N(D−2)+H−2 reaction and its isotopic variants

ARTICLE *in* CHEMICAL PHYSICS · JANUARY 2007

Impact Factor: 1.65 · DOI: 10.1016/j.chemphys.2006.11.032

4 AUTHORS, INCLUDING:

Jesus F Castillo
Complutense University of Madrid
76 PUBLICATIONS **2,062** CITATIONS
SEE PROFILE

Niyazi Bulut
Firat University
40 PUBLICATIONS **281** CITATIONS
SEE PROFILE

Fahrettin Gogtas
Yıldırım Beyazıt Üniversitesi
24 PUBLICATIONS **99** CITATIONS
SEE PROFILE

Available online at www.sciencedirect.com
ScienceDirect
Chemical Physics 332 (2007) 119–131
Chemical Physics
www.elsevier.com/locate/chemphys

Wave packet and quasiclassical trajectory calculations for the $N(^2D) + H_2$ reaction and its isotopic variants

J.F. Castillo [a], N. Bulut [a,1], L. Bañares [a,*], F. Gogtas [b]

[a] Departamento de Química Física, Facultad de Química, Universidad Complutense, 28040 Madrid, Spain
[b] Firat University, Department of Physics, 23169 Elazığ, Turkey

Received 25 September 2006; accepted 29 November 2006
Available online 3 December 2006

Abstract

The $N(^2D) + H_2(v = 0, j = 0)$ reaction and its HD and D_2 isotopic variants have been studied by means of quantum mechanical real wave packet and wave packet with split operator and quasiclassical trajectory methodologies on the potential energy surface of Ho et al. [J. Chem. Phys. 119 (2003) 6]. Total initial state-selected and final state-resolved reaction probabilities and product rotational distributions have been calculated for total angular momentum $J = 0$ in a broad range of collision energies. The real wave packet results are in very good agreement with the corresponding split operator wave packet calculations. A reasonable overall good agreement has been found between the wave packet and quasiclassical trajectory results. Integral cross-sections and thermal rate constants have been calculated from the wave packet reaction probabilities by means of standard J-shifting, refined J-shifting and uniform J-shifting methods in combination with the centrifugal sudden approximation for $J > 0$. Comparisons with available exact wave packet, quasiclassical trajectory and experimental results are made and discussed.

Keywords: Reaction dynamics; Quasiclassical trajectory method; Wave packets; Insertion reactions

1. Introduction

The $N(^2D) + H_2$ elementary reaction is an important step in combustion processes and atmospheric chemistry. Several experimental and theoretical studies of the reaction have been carried out during the last 15 years. Unravelling the mechanism of the title reaction has been a process not exempt of controversy. In the early experimental work by Dodd et al. [1], the vibrational distribution of the nascent NH product was measured by time-resolved infrared emission after a pulsed irradiation of an electron beam against a mixture of N_2 and H_2. The ratio $NH(v' = 1)$:$NH(v' = 2)$:$NH(v' = 3)$ was found to be 1.0:0.97:0.81 and also a $NH(v' = 0)$:$NH(v' = 1)$ ratio of 0.47 was indirectly derived. The measured inverted vibrational population was found to be indicative of a direct abstraction mechanism in a highly exothermic reaction. Kobayashi et al. [2] developed an *ab initio* potential energy surface (PES) for the ground state NH_2 system based on first order configuration interaction (FOCI) calculations. The topology of this PES shows a barrier for the H–N–N linear configuration of 57 meV and a barrier for C_{2v} H–N–H configuration of 21.4 meV in the reactant valley. Subsequent quasiclassical trajectory (QCT) [2] and quantum mechanical (QM) [3] calculations on this PES predicted that the abstraction mechanism was dominant and inverted vibrational distributions of the products were obtained in agreement with experiment.

However, the conclusions drawn from those experimental and theoretical studies were contradicted by newer and more definitive sets of experiments and theoretical works that followed up. First, Umemoto et al. produced $N(^2D)$ atoms by photodissociation of NO and measured the

* Corresponding author. Tel.: +34 913944228.
E-mail address: banares@quim.ucm.es (L. Bañares).
[1] On leave from: Firat University, Department of Physics, 23169 Elazığ, Turkey.

0301-0104/$ - see front matter © 2006 Elsevier B.V. All rights reserved.
doi:10.1016/j.chemphys.2006.11.032

population ratio of vibrational levels of the NH product by laser-induced fluorescence [4–6]. They found that the population of the $v' = 1$ level is little less than that of $v' = 0$ and that the rotational populations of these vibrational states are broad and hot. These observations were quite at odds with the previous experimental [1] and theoretical [2,3] results and they were more consistent with an insertion mechanism for the title reaction. Prompted by the new experiments, Kobayashi and co-workers [7] adjusted empirically their FOCI PES in order to reduce the C_{2v} barrier height and to increase the collinear barrier height. New QCT calculations on the modified PES showed that if insertion dynamics is dominant then the product vibrational distribution is cooler and the rotational distributions hotter than the corresponding distributions in the original FOCI PES [2]. Clearly more detailed experimental and theoretical work was needed to establish the dynamical mechanism of the title reaction on firm grounds.

Important steps for this quest were given by Alagia et al. [8] and Balucani et al. [9] in combined experimental and theoretical studies of the $N(^2D) + D_2$ reaction. Employing the crossed molecular beam (CMB) technique, the angular and velocity distributions of the ND product from the reaction at 0.22 and 0.165 eV collision energies were measured. The center-of-mass product angular distributions were found to be nearly backward–forward symmetric, feature which is characteristic of insertion reactions. At the same time, multireference configuration interaction (MRCI) plus Davidson correction calculations employing the Dunning aug-cc-pVTZ basis set were performed to construct a new PES [10]. The insertion pathway on the new PES has a barrier of 81 meV in C_{2v} geometry and the abstraction path a collinear barrier of 197 meV. Detailed QCT calculations were performed for the $N(^2D) + H_2$ and $N(^2D) + D_2$ reactions and a good agreement was obtained with the experimental product angular and velocity distributions [8] and vibrational distributions of NH [4]. The analysis of the reactive trajectories showed that insertion of the N atom into the H–H bond was the dominant mechanism.

Following those QCT studies, Honvault and Launay [11] performed the first exact QM calculations of the $N(^2D) + H_2$ reaction on the PES of Pederson et al. [10] using a time-independent hyperspherical coordinate method. In their study the $NH(v',j')$ state-resolved integral cross-sections (ICS) and differential cross-sections (DCS) were calculated and compared with the QCT results of Pederson et al. [10] at collision energies of 70, 110 and 165 meV. The QM $NH(v')$ ICS of Honvault and Launay [11] were found to be consistently greater than the QCT ICS's reported by Pederson et al. [10], especially at low collision energies, presumably due to a tunneling effect through the barrier in the entrance arrangement. The corresponding QM DCSs showed a forward–backward symmetry in overall agreement with the QCT DCSs of Pederson et al. [10]. Later on new experiments by Umemoto and co-workers [12] measured the vibrational state distribution of the NH products of the title reaction that agreed well with the exact QM [11] and QCT calculations [10].

The insertion mechanism implies the formation of the NH_2 complex that can live long enough to break up into any accessible reactant or product channel subject to the conservation of total energy and total angular momentum. This statement was proven to be very sound by a QM statistical theory of atom–diatom insertion reactions derived by Rackham et al. [13,14]. This statistical quantum mechanical (SQM) method was rigourously applied to the $N(^2D) + H_2$ reaction [13,14], as well as to other reactions between $C(^1D)$, $O(^1D)$ and $S(^1D)$ with H_2, and the results compared to exact QM reactive scattering calculations by Honvault and Launay. For the case of the $N(^2D) + H_2$ reaction, the total ICSs and the vibrational and rotational distributions calculated using the SQM method [13] were found to be in very good agreement with the exact QM calculations [11]. However, the derived DCSs from the exact QM calculations exhibit a slight forward–backward asymmetry which contrasts with the perfectly symmetric DCSs obtained with the SQM method [14]. The discrepancy was attributed to the fact that the lifetime of the NH_2 complex may not be long enough to decay in a completely statistical way. A more detailed comparison between the experimentally derived angular distributions using the CMB technique and the calculated DCSs obtained by means of QM, QCT and SQM methods on the Pederson et al. PES have been recently carried out by Balucani et al. [15,16].

In a recent work, Ho et al. [17] developed an improved PES for the $1^2A''$ ground state of NH_2 based on the Pederson et al. [10] PES, but with a larger set of *ab initio* points and a better algorithm for fitting the *ab initio* points. The new analytic PES is free from small spurious features and is in better agreement with the *ab initio* points in some key regions including the collinear and C_{2v} barriers, 208 and 78 meV, respectively. The QCT calculations [17] on the improved PES led to thermal rate constants closer to the experimental measurements by Suzuki et al. [18]. Employing this new PES, Bañares et al. [19] performed new QCT and SQM calculations to explore the influence of rotational excitation of the diatom and isotope effects on the dynamics of the title reaction. It was found that rotational excitation of H_2, D_2 and HD increases reactivity in the QCT calculations but in the SQM calculations this effect is much smaller. Interestingly, the SQM rate coefficients for the $N(^2D) + H_2$ and $N(^2D) + D_2$ reactions are somewhat larger than the experimental values [18]. On the same PES, Gogtas and Bulut [20] calculated state-to-state and state-to-all reactive scattering probabilities for $J = 0$ and for the $N(^2D) + H_2(v = 0, j = 0\text{–}2)$ reactions for a broad range of collision energies using a real wave packet (WP) method. The rotationally and vibrationally state-resolved reaction probabilities exhibit many relatively sharp peaks. The first exact ICSs and rate constants for the $N(^2D) + H_2(v = 0, j = 0,\ 2)$ reaction employing the PES by Ho et al. [17] have been calculated by Lin and

Guo [21] using a Chebyshev quantum close-coupling (CC) WP method. The reported exact WP rate coefficients are slightly larger than the experimental data and these exact results show that the QCT method underestimates the exact rate coefficients, while the SQM method somewhat overestimates them.

Very recently, Varandas et al. [22] have produced a new set of *ab initio* points at the MRCI/aug-cc-pVQZ level of theory for the ground state ($1^2A''$) of NH_2. An analytical PES for these *ab initio* point has been obtained by means of the double many-body expansion (DMBE) method. The C_{2v} barrier on this PES is 94 meV (to be compared with the value of 78 meV in the Ho et al. PES [17]). Using this new PES, a very detailed study of the $N(^2D) + H_2$ ($v = 0, j = 0$–5) reaction was performed employing a quantum centrifugal sudden approximation (CSA) WP methodology by Chu et al. [23] and an exact quantum CC WP method by Varandas et al. [24]. Total reaction probabilities, integral cross-sections, and thermal rate constants were computed. It was found that the QM CSA and QM CC WP methods yield practically the same thermal rate constants and are slightly lower than the existing measurements [18].

In this work, we have applied two versions of time-dependent quantum WP methodology, the real WP method of Gray and Balint-Kurti [25] and a complex WP method [26] using the split-operator propagator, along with the QCT method to calculate the reactive scattering of the $N(^2D) + H_2$ and its isotopic variants on the PES by Ho et al. [17]. State-resolved reaction probabilities, product rotational distributions and state-to-all reactive probabilities have been calculated. The cross-sections and thermal rate constants have been obtained via the WP methods using various approximations for $J > 0$: (a) a simple J-shifting method [27] and (b) CSA in combination with J-shifting and uniform J-shifting [28]. The results are compared with QCT results, with the recently available exact WP calculations [21] and with the experimental results. The goals pursued in the present work are twofold: first, the comparison between QM and QCT reaction probabilities can help to identify genuine quantum effects on the dynamics of prototypic insertion reactions and, second, from the comparison between exact QM and approximated QM calculations using the same PES, an assessment of the validity of the approximations can be extracted. The paper is organized as follows: in Section 2 we will review the different theoretical methods employed in this work, Section 3 will present the results and discussion and finally Section 4 will close with the conclusions.

2. Theory

2.1. Real wave packet method

We use the time-dependent real WP method of Gray and Balint-Kurti [25]. As in a previous work [20], the Hamiltonian for $J = 0$ is expressed in product Jacobi coordinates, R_β, r_β, γ_β, as

$$\widehat{H} = \widehat{T} + \widehat{U} \tag{1}$$

where

$$\widehat{T} = -\frac{\hbar^2}{2\mu_R}\frac{\partial^2}{\partial R_\beta^2} - \frac{\hbar^2}{2\mu_r}\frac{\partial^2}{\partial r_\beta^2} \tag{2}$$

and

$$\widehat{U} = -\frac{\hbar^2}{2}\left(\frac{1}{\mu_R R_\beta^2} + \frac{1}{\mu_r r_\beta^2}\right)\frac{1}{\sin\gamma_\beta}\frac{\partial}{\partial\gamma_\beta}\sin\gamma_\beta\frac{\partial}{\partial\gamma_\beta} + V(R_\beta, r_\beta, \gamma_\beta) \tag{3}$$

The basic idea of the real wave packet approach is to map the Hamiltonian operator as

$$f(\widehat{H}) = -\frac{\hbar}{\tau}\cos^{-1}(\widehat{H}_s) \tag{4}$$

where $\widehat{H}_s = a_s\widehat{H} + b_s$ with a_s and b_s chosen to ensure that the minimum and maximum eigenvalues of $\widehat{H}_s$ lie in the interval $(-1,1)$. The WP then evolves under the modified time-dependent Schrödinger equation

$$\mathbf{i}\hbar\frac{\partial\Psi(R_\beta, r_\beta, \gamma_\beta, t)}{\partial t} = f(\widehat{H})\Psi(R_\beta, r_\beta, \gamma_\beta, t) \tag{5}$$

The functional mapping of the Hamiltonian operator allows the propagation of the wave packet to be achieved by a Chebyshev iterative method where each step requires a single evaluation of the action of the Hamiltonian on the real part of the WP [29,30]. If q is the real part of the wave function (ψ) represented on discrete grid points, $q = Re\{\psi\}$, then the propagation is achieved by a damped Chebyshev iteration [31] as

$$q_{n+1} = \widehat{A}(-\widehat{A}q_{n-1} + 2\widehat{H}_s q_n) \tag{6}$$

where n is the iteration step, $n = 1, 2, \ldots, N$. $\widehat{A}$ is a imaginary potential operator for damping the WP at the edges of the grid [32]. This recursion requires q_0 and q_1 to be initialized. q_0 is taken as the real part of the initial WP while q_1 is calculated as

$$q_1 = \widehat{A}[\widehat{H}_s q_0 - \sqrt{1 - \widehat{H}_s^2}p_0] \tag{7}$$

where p_0 is the imaginary part of the initial WP. The action of $\sqrt{1 - \widehat{H}_s^2}$ operator on p_0 is calculated with a Chebyshev polynomial expansion [33]. The initial WP is set up in reactant Jacobi coordinates ($\psi(R_\alpha, r_\alpha, \gamma_\alpha, t = 0)$) and then transformed to product coordinates ($\psi(R_\beta, r_\beta, \gamma_\beta, t = 0)$). The initial wave function has components describing the relative motion of atom A and the vibrational and rotational motions of target molecule BC. This wave function is given an initial momentum in negative R_α direction

$$\psi(R_\alpha, r_\alpha, \gamma_\alpha, t = 0) = \mathrm{e}^{-\mathrm{i}k_0(R_\alpha - R_{0,\alpha})}\mathrm{e}^{-\beta(R_\alpha - R_{0,\alpha})^2} \times \frac{\sin[\alpha(R_\alpha - R_{0,\alpha})]}{R_\alpha - R_{0,\alpha}}\phi_{vj}(r_\alpha)P_j(\cos\gamma_\alpha) \tag{8}$$

where $\phi_{vj}(r_\alpha)$, and $P_j(\cos\gamma_\alpha)$ are the rovibrational and rotational components of the wave function, respectively. $e^{-ik_0(R_\alpha-R_{0,\alpha})}$ gives an initial momentum component to the initial wave function in negative R_α direction. The translational part of the WP has been set up as a Gaussian function multiplied by a sine function as described by Hankel et al. [34]. The rovibrational $\phi_{vj}(r_\alpha)$ eigenfunctions of the diatomic molecule are calculated by using the Fourier Grid Hamiltonian (FGH) Method [35]. Eq. (6) is solved for many iteration steps until the wave function has completely left the interaction region. The reactive S-matrix elements are then given by [25]

$$S_{\beta v',\alpha v}(E) = \frac{\hbar^2 a_s}{\tau(1-E_s^2)^{1/2}}\left(\frac{k_{\beta v'}k_{\alpha v}}{\mu_{A-BC}\mu_{AB-C}}\right)^{1/2} \times \exp(-ik_{\beta v'}R_\infty)\frac{2A_{\beta v',\alpha v}(f)}{g(-k_{\alpha v})} \quad (9)$$

where $v = v, j$, $v' = v', j'$, τ is time step for propagation and $E_s = a_s E + b_s$. The energy dependent amplitudes, $A_{\beta v',\alpha v}(f)$, are the Fourier transform of the time dependent coefficients

$$C_{\beta v',\alpha v}(t) = \int_{r=0}^{\infty} q(R_\infty, r, \gamma, t)\phi_{v'j'}(r)\,dr \quad (10)$$

while $g(-k_{\alpha v})$ is the Fourier transform of the gaussian component of the initial wave packet.

2.2. Wave packets using split operator method

Another time-dependent WP method for state-to-state reactive scattering is based on the following expression for the reactive scattering matrix elements, $S_{\beta v',\alpha v}(E)$, involving the Fourier transform of a correlation function, $C_{\beta v',\alpha v}(t)$, between an initial reactant wave packet $\chi_{\alpha v}$ and a final product wave packet $\chi_{\beta v'}$ [26]:

$$S_{\beta v',\alpha v}(E) = -\frac{1}{\langle\chi_{\beta v'}|\phi^+_{E\beta v'}\rangle\langle\phi^-_{E\alpha v}|\chi_{\alpha v}\rangle}\int_0^\infty e^{+iEt/\hbar}C_{\beta v',\alpha v}(t)\,dt, \quad (11)$$

where

$$C_{\beta v',\alpha v}(t) = \langle\chi_{\beta v'}|e^{-i(H-i\epsilon)t/\hbar}|\chi_{\alpha v}\rangle \quad (12)$$

and $\phi^\pm_{E\gamma v''}$ ($\gamma = \alpha$, β and $v'' = v$, v') are energy normalized incoming and outgoing waves in the corresponding channels. The small but finite ϵ term ensures the convergence of the time integral. A number of different derivations of this expression have been given in the last few years, ranging from the straightforward derivation given by Dai and Zhang [36] to the more formal derivation given by Tannor and Weeks [37].

In this work, we use the mass-scaled Jacobi coordinates R_α, r_α, and γ_α of the reactant arrangement [38], in terms of which the Hamiltonian $\widehat{H}$ for total angular momentum $J = 0$ is given by [39]

$$\widehat{H} = \widehat{T} + \widehat{U} \quad (13)$$

where

$$\widehat{T} = -\frac{\hbar^2}{2\mu}\left(\frac{\partial^2}{\partial R_\alpha^2} + \frac{\partial^2}{\partial r_\alpha^2}\right) \quad (14)$$

and

$$\widehat{U} = -\frac{\hbar^2}{2\mu}\left(\frac{1}{R_\alpha^2} + \frac{1}{r_\alpha^2}\right)\frac{1}{\sin\gamma_\alpha}\frac{\partial}{\partial\gamma_\alpha}\sin\gamma_\alpha\frac{\partial}{\partial\gamma_\alpha} + V(R_\alpha, r_\alpha, \gamma_\alpha) \quad (15)$$

The incoming and outgoing waves $\phi^\pm_{E\gamma v''}$, with $\gamma = \alpha$, β and $v'' = v\ j, v'j'$, are defined as

$$\phi^\pm_{E\gamma v''} = v^{-1/2}_{E\gamma v''}h^{(2)}_j(k_{E\gamma v''}R_\gamma) \quad (16)$$

where $h^{(2)}_{j''}(k_{E\gamma v''}R_\gamma) \sim \exp[\pm i(k_{E\gamma v''} - j''\pi/2)]$, with $j'' = j,\ j'$, is a Ricatti–Hankel function with $k_{E\gamma v''} = \sqrt{2\mu(E - E_{\gamma v''})}/\hbar)$ as the asymptotic wave number and $v = \hbar k_{E\gamma v''}/\mu$ as the asymptotic velocity in channel $\gamma v''$. The initial reactant and final product wave packets $\chi_{\gamma v''}$ are defined as

$$\chi_{\gamma v''} = \frac{1}{R_\gamma r_\gamma}e^{-(R_\gamma - R_{0,\gamma})^2/2\delta^2 - ik_{\gamma,0}R_\gamma}\phi_{v''}(r_\gamma)P_{j''}(\cos\gamma_\gamma) \quad (17)$$

The Hamiltonian $\widehat{H}$ has been represented using discrete variable representations (DVRs) for the radial coordinates, R_α and r_α, and a Legendre polynomial basis set is used to describe the angular coordinate, γ_α. Gauss–Legendre quadrature points are employed as angular grid points [40]. Using the above representation, the final product wavepackets $\chi_{\beta v'}$ are calculated in the reactant grid representation as

$$\langle R_\alpha, r_\alpha, \gamma_\alpha|\chi_{\beta v'}\rangle = \Delta R_\alpha^{1/2}\Delta r_\alpha^{1/2}\omega_\alpha^{1/2}\frac{R_\beta r_\beta}{R_\alpha r_\alpha}e^{(R_\beta - R_{0,\beta})^2/2\delta^2 - ik_{\beta,0}R_\beta} \times \phi_{v'}(r_\beta)P_{j'}(\cos\gamma_\beta) \quad (18)$$

The Hamiltonian matrix in the present representation is very sparse. Therefore, the time evolution of the wave packet can be performed using the split operator method [41] with a partitioning of the evolution operator as

$$e^{-i\widehat{H}\Delta t/\hbar} = e^{-i\widehat{U}\Delta t/2\hbar}e^{-i\widehat{T}\Delta t/\hbar}e^{-i\widehat{U}\Delta t/2\hbar} + O(\Delta t^3) \quad (19)$$

A complex absorbing potential $V_{opt}(R_\alpha, r_\alpha)$ has been incorporated to absorb the wave packet over the last quarter of the DVR grids in R_α and r_α.

2.3. Approximations for $J > 0$

A quite approximate way to estimate reaction probabilities for $J > 0$ is by using standard J-shifting methodologies. The $N(^2D) + H_2$ PES have collinear and C_{2v} barriers in the entrance channel. The existence of a barrier in the PES allow us to use the simple J-shifting method of Bowman [27]. In the standard J-shifting method, initial v, j state-specific total reaction probabilities for $J > 0$ are calculated by using

$$P^J_{vj}(E_c) \approx P^{J=0}_{vj}[E_c - E^J_{shift}] \quad (20)$$

where $P_{vj}^{J=0}$ is the initial v, j quantum state-resolved reaction probability for $J = 0$ as a function of collision energy E_c, and $P_{vj}^{J}(E_c)$ is the estimated reaction probability for a higher value of J at energy $E_c - E_{shift}^{J}$. In the C_{2v} transition state of the NH_2 system, the moments of inertia are $I_a^{\ddagger} < I_b^{\ddagger} \approx I_c^{\ddagger}$ (nearly a prolate symmetric top), so the shifting energy can be defined as (for the case of $K = 0$)

$$E_{shift}^{J} = \frac{1}{2}(B^{\ddagger} + C^{\ddagger})J(J+1) \tag{21}$$

However, this definition of E_{shift}^{J} is not valid for the collinear NH_2 transition state. Thus, at collision energies above 0.2 eV (the value of the linear energy barrier), we have employed the following definition

$$E_{shift}^{J} = \frac{\hbar^2}{2\mu_R R_0^2}J(J+1) \tag{22}$$

where R_0 and μ_R are the A–BC distance at the transition state and reduced mass, respectively.

A better approach is to employ the centrifugal sudden approximation (CSA) for dynamical calculations at $J > 0$, which significantly reduces the amount of computational effort [42] with respect to the exact coupled-channel (CC) calculations. Recently, CSA and CC calculations of reaction probabilities for high Js have been performed by Chu et al. [23] for the $N(^2D) + H_2$ reaction, proving that the CSA method yield results very close to the CC method.

Once the $P_{v,j}^{J}(E_c)$ are obtained, total integral cross-sections are calculated by summing the partial cross-sections over all J values as

$$\sigma_{v,j}(E_c) = \frac{\pi}{k_{v,j}^2}\sum_{J=0}(2J+1)P_{v,j}^{J}(E_c) \tag{23}$$

The v, j state-specific rate constant can be calculated by Boltzmann averaging of the corresponding integral cross-section $\sigma_{v,j}(E_c)$ over collision energy as

$$k_{v,j}(T) = \left(\frac{8}{\pi\mu_R(k_B T)^3}\right)^{1/2}\int_0^{\infty} E_c\sigma_{v,j}(E_c)e^{-E_c/k_B T}\,dE_c \tag{24}$$

where k_B is the Boltzmann constant and E_c is the collision energy.

Another very appealing method for evaluating reaction rate constants is the Uniform J-shifting (UJS) approach developed by Zhang and Zhang [28]. In this case, the rate constant is given by

$$k_{UJS}(T) = \sqrt{\frac{2\pi}{(\mu_R k_B T)^3}}Q^0(T)\sum_J(2J+1)e^{-B_i(T)J(J+1)/k_B T} \tag{25}$$

where

$$Q^0(T) = \int P^0(E_c)e^{-E_c/k_B T}\,dE_c, \tag{26}$$

$$B_i(T) = \frac{k_B T}{J_{i+1}(J_{i+1}+1) - J_i(J_i+1)}\ln\left(\frac{Q^{J_i}}{Q^{J_{i+1}}}\right)(i = 1,2) \tag{27}$$

and

$$Q^J(T) = \int P^J(E_c)e^{-E_c/k_B T}\,dE_c \tag{28}$$

This method requires to calculate at least the total reaction probabilities for three values of J and can be generalized to cases with more than three values of J. Chu et al. [23] used this UJS approach in combination with CSA for the $N(^2D) + H_2$ reaction, obtaining rate constants in excellent agreement with those calculated by computing CSA reaction probabilities for all Js up to convergence.

2.4. Quasiclassical trajectory calculations

The quasiclassical trajectory method used for the calculations presented here has been described in previous publications (see, for instance, Ref. [43] and references therein) and only the details relevant to the present work will be given here.

For the present work, batches of 2×10^5 trajectories were run on the $1^2A''$ PES of Ho et al. [17] for initial rotational state $j = 0$ and total angular momentum $J = 0$ (zero impact parameter) for randomly sampled collision energies, E_c, between threshold and 1.0 eV for all isotopic variants of the reaction, $N(^2D) + H_2$, $N(^2D) + D_2$ and $N(^2D) + HD$. Trajectories were started at a $N(^2D)$–$H_2(D_2, HD)$ distance of 8 Å and a time step of 0.05 fs was used for the integration of the equations of motion. Under these conditions total energy was conserved to better than 1 part in 10^4.

The calculation of the total and vibrationally state-resolved reaction probabilities for $J = 0$ were performed by the method of moments expansion in Legendre polynomials [43].

3. Results and discussion

In what follows, we will refer to the real wave packet method as RWP and to the wave packet method using split-operator as SWP. The most relevant parameters used in the RWP and SWP calculations are given in Tables 1 and 2, respectively.

Table 1
Parameters used in the RWP calculations (all parameters are given in atomic units)

Scattering coordinate range	$R_{min} = 0.0$; $R_{max} = 12.5$
Number of grid points in R	127
Diatomic coordinate range	$r_{min} = 0.9$; $r_{max} = 11.5$
Number of grid points in r	119
Number of angular basis functions	60
Center of initial wave packet	$R_0 = 6.0$
Gaussian width factor	$\beta = 0.5$
Smooth parameter	$\alpha = 1.5$
Initial wave vector	$k_0 = 7.7$
Position of analysis line	$R_\infty = 8.0$
Number of Chebyshev iterations	40,000

Table 2
Parameters used in the SWP calculations (all parameters are given in atomic units)

Scattering coordinate range	$R_{min} = 0.0$; $R_{max} = 15.0$
Number of grid points in R	259
Diatomic coordinate range	$r_{min} = 0.0$; $r_{max} = 15.0$
Number of grid points in r	259
Number of angular basis functions	300
Center of initial wave packet	$R_0 = 10.9$
Center of products wave packets	$R_0 = 10.9$
Gaussian width factor	$\delta = 0.17$
Average wave vector of initial wave packet	$k_0 = 8.2$
Average wave vector of final wave packets	$k_0 = 8.2$
Truncation parameter for DVR grid	$V_{max} = 0.044$
Time step for propagation	$\Delta t = 3.3$ (0.08 fs)
Propagation time	40,000 (960 fs)

3.1. Reaction probabilities

Fig. 1 shows RWP, SWP and QCT total reaction probabilities for $J = 0$ as a function of collision energy, $P^{J=0}(E_c)$, for the $N(^2D) + H_2$ (top panel) and $N(^2D) + D_2$ (bottom panel) reactions with the reagents in the $v = 0, j = 0$ ground state. As can be seen, all calculated $P^{J=0}(E_c)$ show a threshold followed by a fast rise and a level off at collision energies larger than about 0.15 eV, in agreement with previous theoretical calculations on previous PESs [14].

As expected, both wave packet methods, RWP and SWP, yield very similar results with reaction probabilities showing broad oscillations after the threshold. The exception to this behavior is the sharp peak feature at ≈0.08 eV collision energy for the reaction with H_2 molecules. A similar peak has been observed also by Lin and Guo [21] in their wave packet calculations on the same PES. We should recall that the ground state NH_2 PES used in the present work has classical barriers of 0.078 eV and 0.21 eV in the entrance channel for C_{2v} and collinear configurations, respectively. This first peak near threshold in the wave packet reaction probabilities could be attributed to a shape resonance in the C_{2v} transition state. In fact, for the $N(^2D) + D_2$ reaction this first peak is significantly smaller (about 25%) and appears at a slightly lower collision energy (≈0.07 eV) than that observed for $N(^2D) + H_2$. This shifting to lower collision energies and the reduction of the height of the peak clearly indicate an

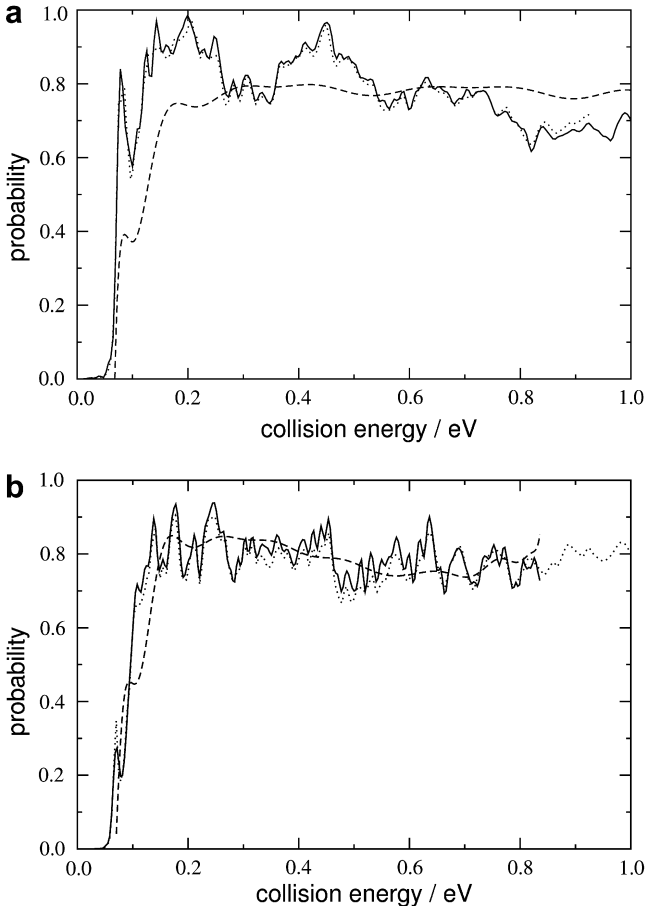

Fig. 1. (a) Total reaction probabilities for total angular momentum $J = 0$ as a function of collision energy for the $N(^2D) + H_2$ ($v = 0, j = 0$) reaction calculated on the PES by Ho et al. [17]. Solid line, RWP; dotted line, SWP; dashed line, QCT. (b) Same as (a) but for the $N(^2D) + D_2$($v = 0, j = 0$) reaction.

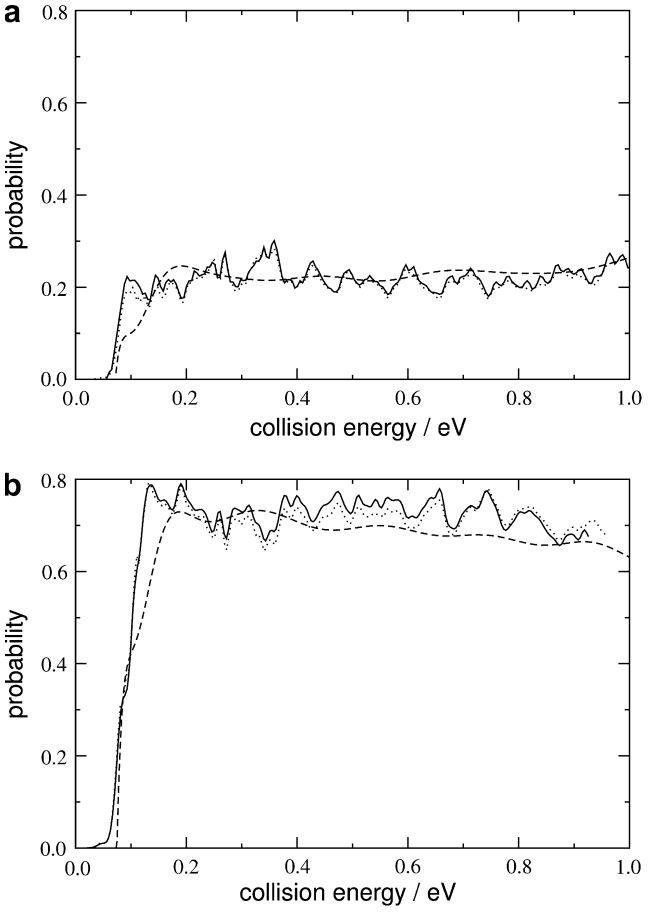

Fig. 2. Total reaction probabilities at $J = 0$ as a function of collision energy for the two-channel $N(^2D) + HD(v = 0, j = 0)$ reaction. (a) Channel NH + D. Solid line, RWP; dotted line, SWP; dashed line, QCT. (b) Same as (a) but for the ND + H channel. All calculations carried out on the PES by Ho et al. [17].

isotopic effect. The probability of tunnelling through the potential barrier in the case of the heavier ND_2 system should be smaller compared to the lighter NH_2 system. Besides the energy of the quasi-bound or resonant state must be lower for the N–D–D complex than for the N–H–H complex.

The QCT $P^{J=0}(E_c)$ are depicted also in Fig. 1 and are found to be in a good qualitative agreement with the WP results. QCT reaction thresholds for both isotopic variants are somewhat larger than the wave packet ones and the $P^{J=0}(E_c)$ curves show significantly less structure. Interestingly, the QCT $P^{J=0}(E_c)$ for the $N(^2D) + H_2$ reaction exhibits a small peak at ≈0.08 eV, which resembles that found in the wave packet calculations commented on above. The corresponding QCT $P^{J=0}(E_c)$ for $N(^2D) + D_2$ show as well a peak at ≈0.09 eV, but in this case, its maximum is somewhat higher than that observed for the $N(^2D) + H_2$ reaction. The origin of this peak in the QCT $P^{J=0}(E_c)$ is not clear. For $N(^2D) + H_2$, reaction probability goes from 0.3932 at the maximum of the peak ($E_c = 0.0863$ eV) to 0.38814 at the minimum ($E_c = 0.1015$ eV) before it rises again. An analysis of trajectories in terms of their collision times [44,45] at fixed collision energies in the vicinity of the maximum shows that right in the minimum there is a decrease in the number of trajectories with collision times in the range 70–100 fs appearing in the forward scattering hemisphere. After the minimum, those trajectories appear again and, in addition, abstraction trajectories with collision times below 50 fs start to appear too. Thus, it is evident that the peak structure in the $P^{J=0}(E_c)$ is related with a change in the reaction mechanism occurring in this collision energy range. Whether this is related with the QM interpretation in terms of a resonance would require further analysis.

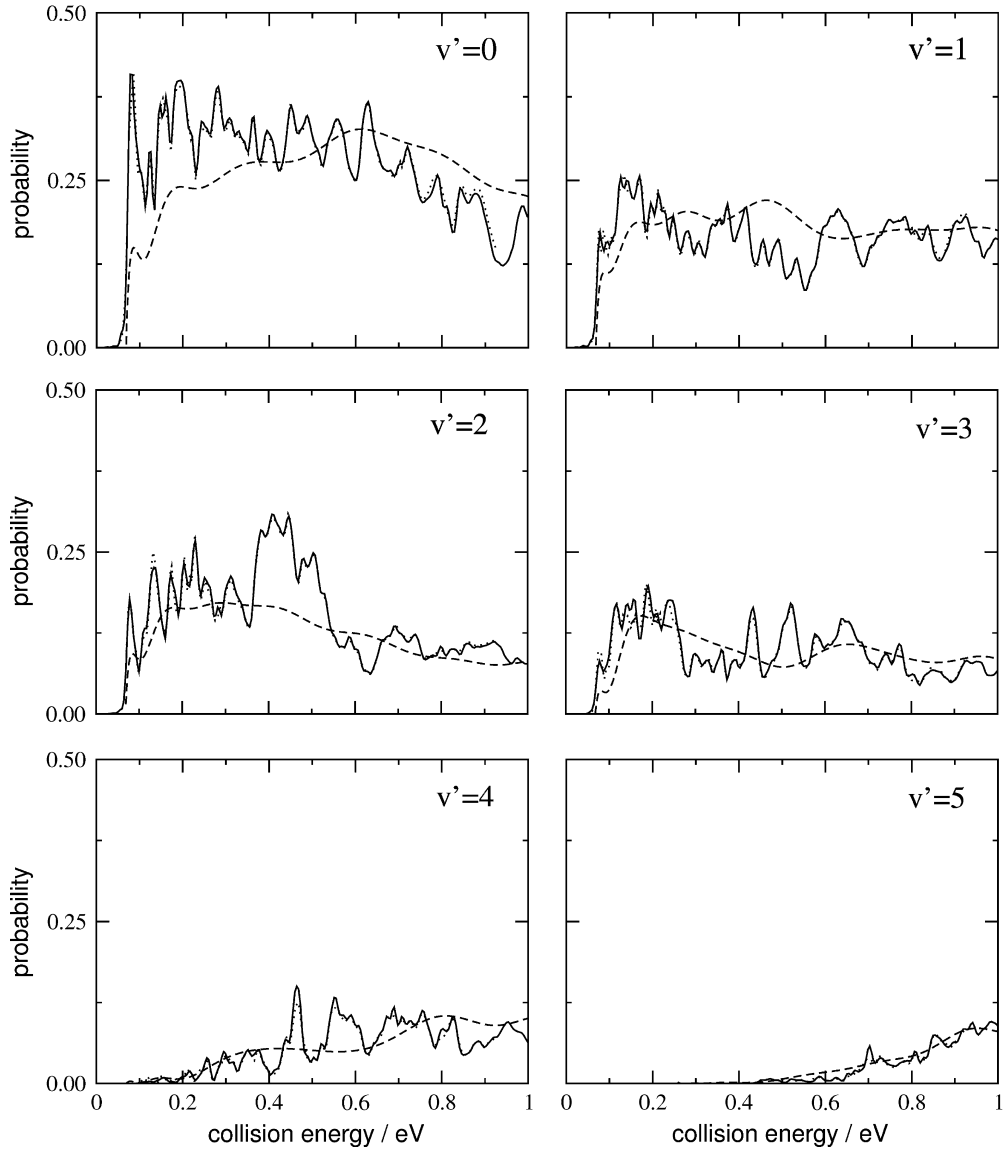

Fig. 3. Vibrationally state-resolved reaction probabilities at $J = 0$ as a function of collision energy for the $N(^2D) + H_2(v = 0, j = 0)$ reaction. Solid line, RWP; dotted line, SWP; dashed line, QCT.

Fig. 2 shows RWP, SWP and QCT $P^{J=0}(E_c)$ for the two channels of the $N(^2D) + HD(v = 0, j = 0)$ reaction. The reaction probabilities for the ND + H channel (lower panel) are significantly larger than those for the NH + D channel. This difference in reactivity between the two channels of the $N(^2D) + HD$ reaction has been discussed in a previous work [19] and it has been attributed to the asymmetric location of the center-of-mass of the HD diatom. The total reaction probabilities obtained by adding the contribution of the two channels are very similar to those of the $N(^2D) + H_2$ and $N(^2D) + D_2$ reactions. In this case, however, the isolated peak found in the WP $P^{J=0}(E_c)$ for the $N(^2D) + H_2$ and $N(^2D) + D_2$ reactions is not clearly seen. For the NH + D channel, the first peak becomes broader and it is shifted towards slightly higher collision energies. For the ND + H channel, the peak gets also broader and can only be appreciated as a shoulder in the rise of the reaction probability at a collision energy of ≈0.07 eV. The agreement between the QCT and WP $P^{J=0}(E_c)$ is also good for the two channels of this isotopic variant. Once again QCT thresholds are somewhat higher and smoothers curves are obtained in comparison with the WP results.

The good agreement found between the two WP methods and the QCT approach extends also to the vibrationally state-resolved reaction probabilities at $J = 0$, as shown in Fig. 3 for the $N(^2D) + H_2(v = 0, j = 0)$ reaction. It is interesting to see how the threshold to reaction increases for the largest v' states in the RWP and SWP results and how this behavior is well reproduced by the QCT calculations. In general, the v' state-resolved WP reaction probabilities show more structure than the total one, especially for low values of v'. The first isolated peak in the total $P^{J=0}(E_c)$ commented on above is most prominent in the $v' = 0$ reaction probabilities, but it has also contributions at the higher $v' = 1$, 2 and 3 states. An analysis

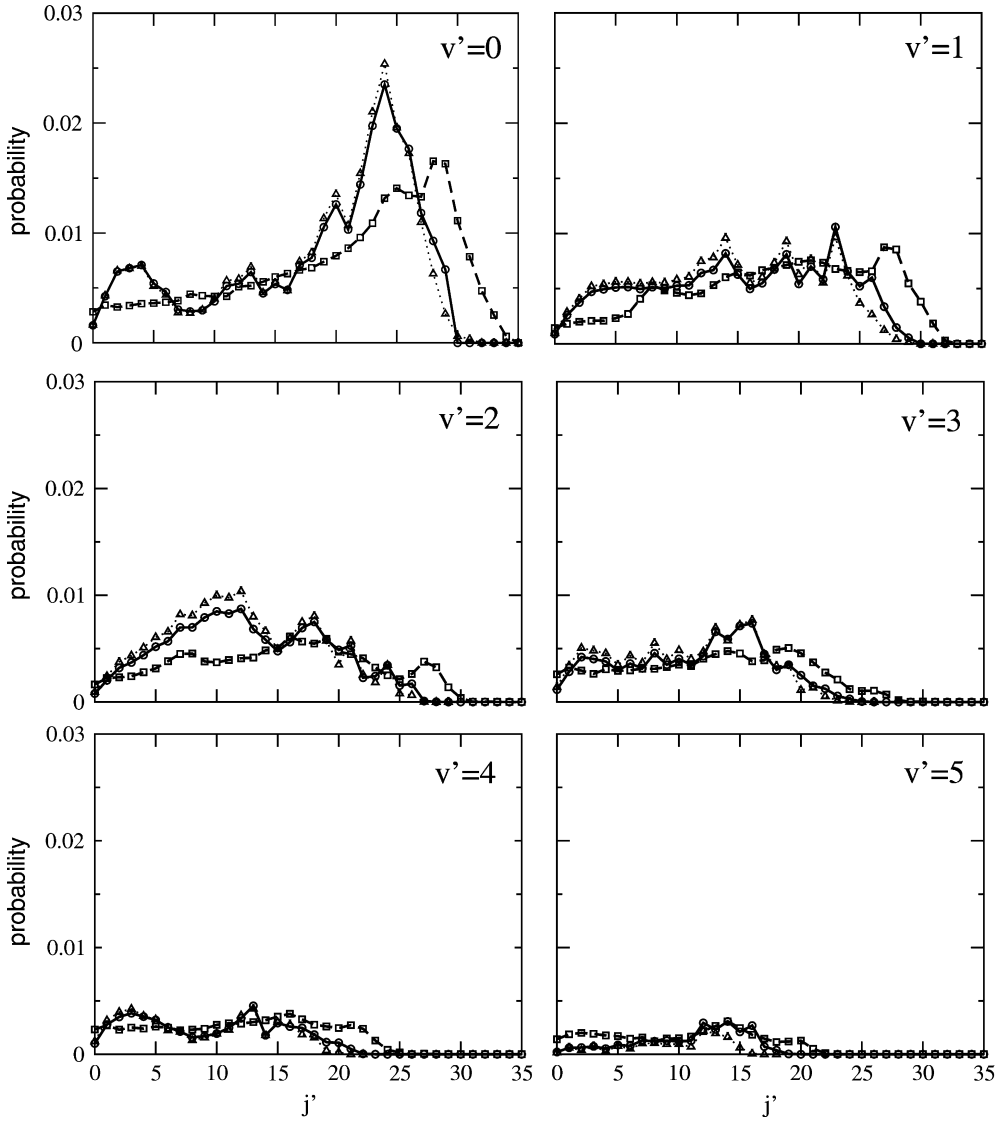

Fig. 4. Final v', j' state-resolved reaction probabilities at $J = 0$ averaged over the collision energy range from threshold up to 1 eV for the $N(^2D) + H_2(v = 0, j = 0)$ reaction. Solid line with circles, RWP; dotted line with triangles, SWP; dashed line with squares, QCT.

of the rotationally state-resolved reaction probabilities for HD products in $v' = 0$ indicates that the isolated peak is more pronounced at low j' states which further supports the interpretation of this peak as a shape resonance. An even better agreement between WP and QCT results for v' state-resolved reaction probabilities is found for the other isotopic variants of the reaction (not shown).

Fig. 4 shows the rotational reaction probability distributions for the different product vibrational states of the $N(^2D) + H_2(v = 0, j = 0)$ reaction averaged over the range of calculated collision energies. Again the agreement between the RWP and SWP results is excellent for every v', j' state. The corresponding QCT calculations yield rotational distributions that extend to slightly higher j' states, especially for $v' = 0$ and $v' = 1$, but agree in general very nicely with the WP results. Similar degree of agreement between RWP, SWP and QCT is also found for the $N(^2D) + D_2$ and the two-channel $N(^2D) + HD$ reactions (not shown).

We have applied the CSA to calculate reaction probabilities for $J > 0$. Fig. 5 displays the results obtained for the $N(^2D) + H_2(v = 0, j = 0)$ and $N(^2D) + D_2(v = 0, j = 0)$ reactions at $J = 5$, 10, 15, 20, 25 and 30, calculated from the corresponding SWP $P^{J=0}(E_c)$ using the CSA. As can be seen, as J increases, both $P^{J>0}(E_c)$ shift towards larger collision energies, but the main features of the $P^{J=0}(E_c)$ are retained for all values of J. These CSA $P^{J>0}(E_c)$ have been used to calculate ICSs as a function of collision energy as we will show in the next section.

3.2. Integral cross-sections

WP integral cross-sections have been calculated by applying various versions of the J-shifting approximation and the CSA approximation as detailed in Section 2.3.

Excitation functions, $\sigma(E_c)$, i.e. the ICS as a function of collision energy, for the $N(^2D) + H_2(v = 0, j = 0)$ and $N(^2D) + D_2(v = 0, j = 0)$ reactions calculated by applying the different approximations are depicted in Fig. 6, along with the existing QCT [19] and exact WP [21] results obtained on the same PES. As can be seen, the simple J-shifting approximation underestimates the ICSs when compared to the exact WP results at collision energies

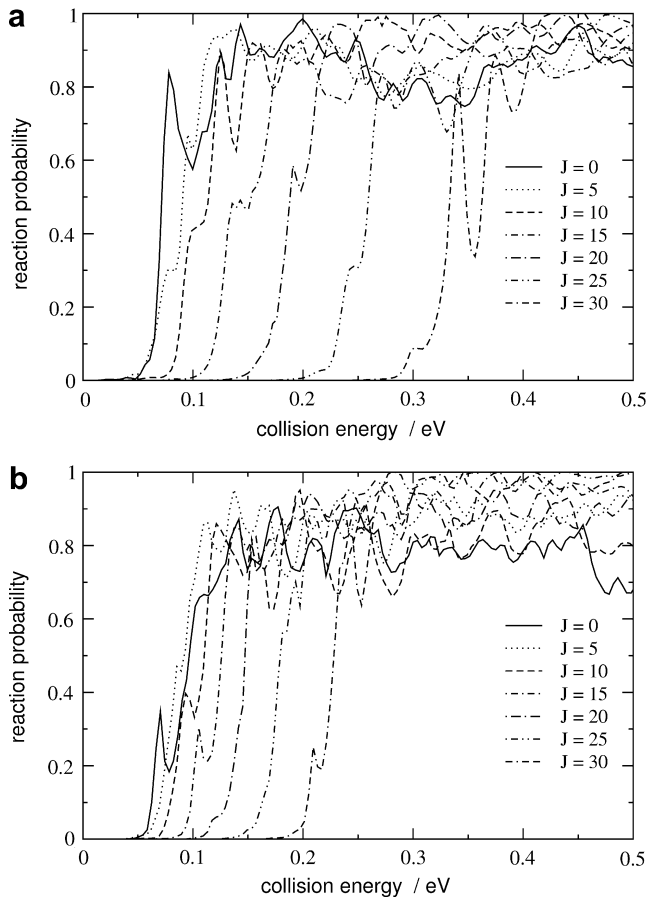

Fig. 5. Total reaction probabilities as a function of collision energy calculated using the centrifugal sudden approximation (CSA) and the SWP method for $J = 5$, 10, 15, 20, 25 and 30. (a) $N(^2D) + H_2(v = 0, j = 0)$ reaction. (b) $N(^2D) + D_2(v = 0, j = 0)$ reaction.

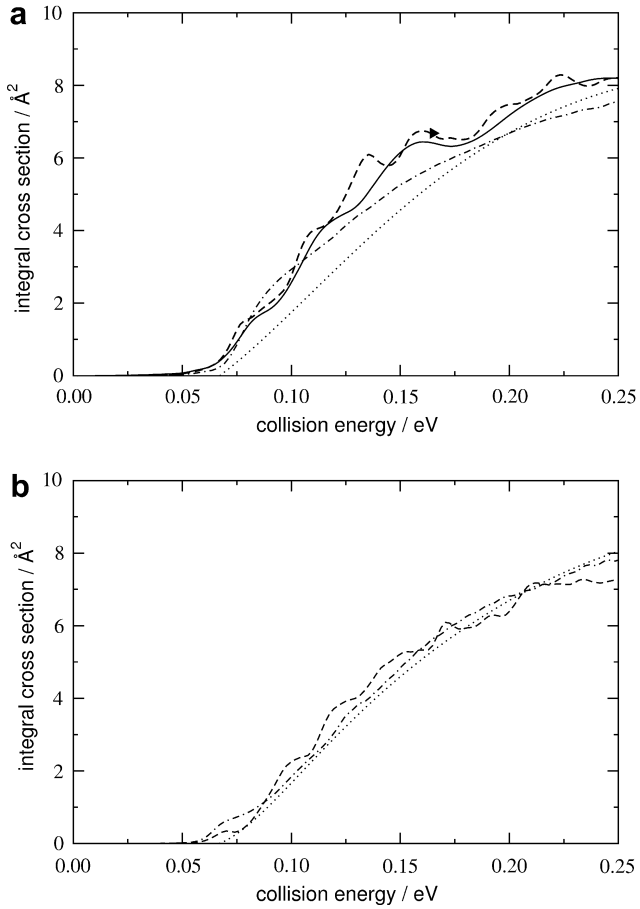

Fig. 6. Integral cross-sections as a function of collision energy. (a) $N(^2D) + H_2(v = 0, j = 0)$ reaction. Solid line, exact WP results from Ref. [20]; dot-dashed line, WP JS; dashed line, WP CSA + Ref-JS; dotted line, QCT from Ref. [19]; solid triangle, exact time-independent QM result from Ref. [11]. (b) $N(^2D) + D_2(v = 0, j = 0)$ reaction. Solid line, WP JS; dashed line, QCT from Ref. [19].

above 0.1 eV and cannot reproduce the wide oscillations in the $\sigma(E_c)$ obtained in that calculation.

A more refined J-shifting approach has been applied by using the specific reaction probabilities obtained within the CSA approximation for $J = 0$, 5, 10, 15, 20, 25 and 30. We have calculated specific B_i constants to estimate the reaction probabilities between the intervals $J = 0$ and 5, $J = 5$ and 10, $J = 10$ and 15 and so on. As can be seen, the $\sigma(E_c)$ obtained by using this CSA J-shifting scheme is in better agreement with the exact WP result. Note that both excitation functions show similar oscillations. In addition, the CSA ICS at $E_c = 0.165$ eV compares very well with the exact time-independent QM ICS calculated in Ref. [11] (this last ICS was obtained on the PES of Pederson et al. [10]; however, it is expected that the differences in the values of the ICSs obtained on both versions of the PES are not very large [17]). The QCT excitation function is always below the exact WP and the refined J-shifting ones, which indicates that quantum effects such tunnelling can be important in the range of collision energies considered in this work. The J-shifting and QCT $\sigma(E_c)$ for the $N(^2D) + D_2(v = 0, j = 0)$ reaction are depicted in the bottom panel of Fig. 6. For this isotopic variant, the simple and CSA J-shifting $\sigma(E_c)$ are in very good agreement with the QCT results, since for this isotopic variant tunneling effects are expected to be less important.

Fig. 7 compares v' state-resolved ICSs calculated with the CSA J-shifting method with QCT and the exact time-independent QM calculations of Honvault and Launay [11] calculated on the PES by Pederson et al. [10]. The agreement between the CSA J-shifting and exact time-independent QM results is rather good. The QCT ICSs show the same behavior, but their values are somewhat smaller.

Fig. 8 presents the simple J-shifting and QCT $\sigma(E_c)$ for the NH + D and ND+H channels of the $N(^2D) + HD$ $(v = 0, j = 0)$ reaction. For the NH + D channel, the QCT $\sigma(E_c)$ is noticeably smaller than the J-shifting one at collision energies below ≈0.2 eV. Tunneling of the H-atom through the C_{2v} barrier in the entrance channel would be a likely effect responsible for the discrepancy. As expected, the agreement between simple J-shifting and QCT methods is found to be much better for the ND + H channel.

3.3. Rate constants

The rate constants calculated for the $N(^2D) + H_2$ $(v = 0, j = 0)$ reaction using the SWP $J = 0$ results and different J-shifting and CSA approximations are plotted in Fig. 9 along with the available exact WP [21], QCT [19] and experimental data [18]. All the theoretical rate constants shown in the figure have been calculated on the same PES. The simplest approximation is to make a Boltzmann integration over collision energy of the excitation function calculated using the standard J-shifting approach, which

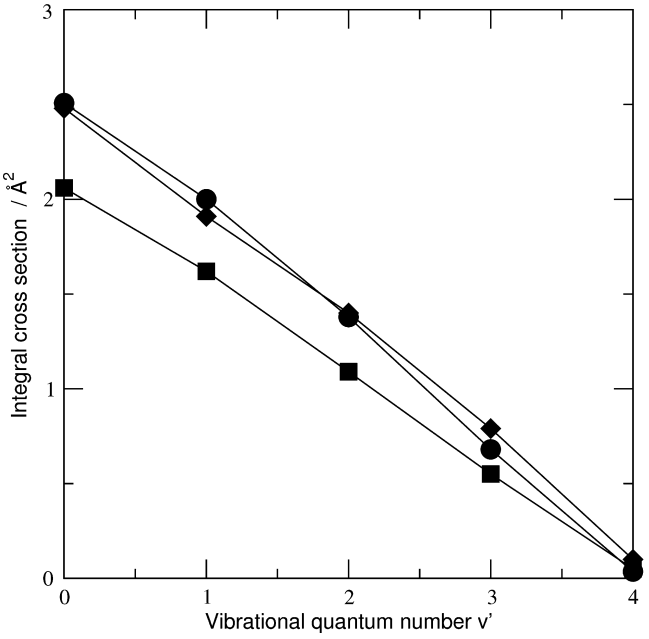

Fig. 7. Integral cross-sections as a function of vibrational quantum number v' for the $N(^2D) + H_2(v = 0, j = 0)$ reaction at $E_c = 0.165$ eV. Solid diamonds, exact time-independent QM results from Ref. [11]; Solid circles, WP CSA + Ref-JS; Solid squares, QCT results from Ref. [17].

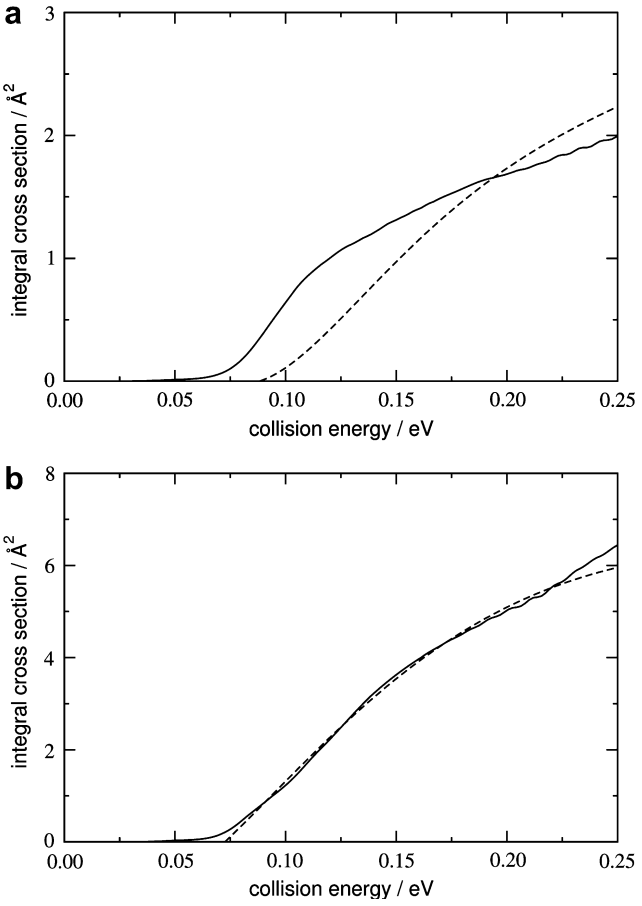

Fig. 8. Integral cross-sections as a function of collision energy for the two-channel $N(^2D) + HD(v = 0, j = 0)$ reaction. (a) NH + D channel. (b) ND + H channel. Solid line, WP JS; dashed line, QCT from Ref. [19].

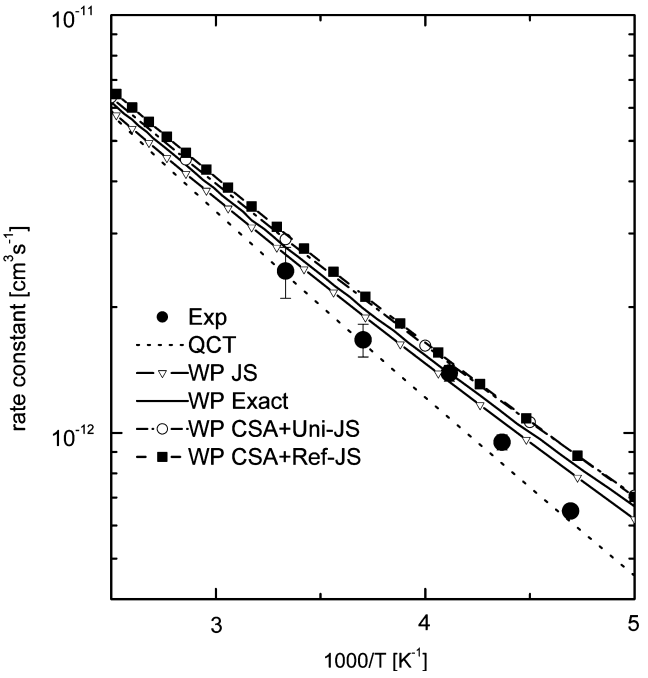

Fig. 9. Rate constants for the $N(^2D) + H_2(v = 0, j = 0)$ reaction. Closed symbols, experimental results from Ref. [18]; dashed line, QCT from Ref. [19]; solid line, exact WP results from Ref. [20]; solid line with down-triangles, WP JS; dashed line with circles, WP CSA + Uni-JS; dashed line with solid squares, WP CSA + Ref-JS.

we have denoted WP JS. Analogously, we have calculated the rate constants using the excitation function obtained with the CSA J-shifting scheme described above (denoted WP CSA + Ref-JS). Finally, the uniform J-shifting approach of Zhang and Zhang [28] has been used to calculate the rate constants from the reaction probabilities obtained with the CSA and SWP methods at $J = 0$, 5, 10, 15, 20 and 30 (denoted WP CSA + Uni-JS).

As can be seen, the three approximate methods yield rate constants in good agreement with the exact WP calculations. However, whereas the WP JS rate constants are smaller than the exact ones, both the WP CSA + Ref-JS and WP CSA + Uni-JS methods predict somewhat larger values. In all cases, the experimental data lie slightly below the exact and approximate WP rate constants. We must notice that the exact and approximate WP calculations have been carried out for the reaction with H_2 in $v = 0$, $j = 0$. However, we are confident in the comparison with the thermal rate constant measurements because it has been shown recently [19,21] that the effect of H_2 rotation on reactivity is very small in the QM calculations carried out for this reaction. The QCT rate constants from Ref. [19] are also below all the WP calculations and seem to match better the experimental results. This is an indication that the angular and collinear barriers of the Ho et al. PES are somewhat too low.

In fact, the recent accurate CC WP calculations by Varandas et al. [24] on the new DMBE PES for this same reaction predict rate constants lower than the experimental results. This DMBE PES has a C_{2v} barrier of 93 meV, which is 15.6 meV higher than that of the Ho et al. PES [17]. Most probably, it is this small difference in the height of the C_{2v} barrier on the two PESs what can account for the discrepancy between the two CC WP calculations. Varandas et al. claim that the barriers of the DMBE PES are more accurate than all previous determinations, including those of Ho et al. for the PES used in the present work. The use of a aug-cc-pVQZ basis in the MRCI calculation seems to be crucial for an accurate determination of the barrier heights. If this is the case, then the best PES is predicting too low rate constants when accurate CC WP calculations are carried out and this would open the possibility of the participation in the reaction of excited PESs.

Fig. 10 shows the calculated rate constants for the $N(^2D) + D_2$ reaction using the SWP method in combination with the different J-shifting methods commented on above along with the experimental measurements and the QCT results from Ref. [19]. The approximate WP rate constants are in very good agreement with experiment and

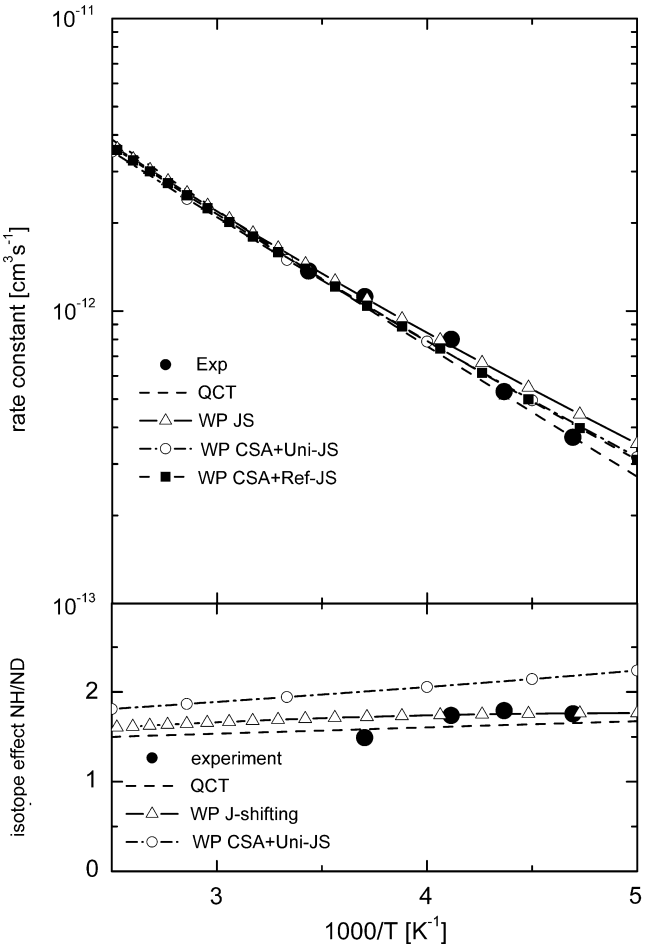

Fig. 10. (Top panel) Rate constants for the $N(^2D) + D_2(v = 0, j = 0)$ reaction. (Bottom panel) Intermolecular isotope effect NH/ND for the $N(^2D) + D_2(v = 0, j = 0)$ and $N(^2D) + H_2(v = 0, j = 0)$ reactions. Closed symbols: experimental results from Ref. [18]. Dashed lines, QCT results from Ref. [19]; solid line with up-triangles, WP JS; dot-dashed line with open circles, WP CSA + Uni-JS; dashed line with closed squares, WP CSA + Ref-JS.

QCT for this isotopic variant. The intermolecular NH/ND isotope effect for the $N(^2D) + H_2$ and $N(^2D) + D_2$ reactions is displayed in the bottom panel of Fig. 10. The WP JS and QCT isotope effect agree very well with the experimental values. However, the WP CSA + Uni-JS method predicts isotope effect larger than experiment. As pointed out in Ref. [19], these values of the NH/ND isotopic ratio are essentially due to the higher collision frequency of $N(^2D) + H_2$, since the cross-sections for the reactions with H_2 and D_2 are very similar. Assuming a line-of-centers functionality for $\sigma(E_c)$, which should be a good approximation for the post-threshold region, a value of 1.33 for the NH/ND branching ratio is predicted [19], not too far from the calculated ones. With decreasing temperatures, the WP CSA + Uni-JS ratio grows slightly faster than the QCT one, possibly due to the contribution of tunnelling, which should be more pronounced for the lighter $N(^2D) + H_2$ isotopic variant.

Fig. 11 shows the rate constants for each of the two output channels of the $N(^2D) + HD$ reaction calculated with SWP and the simple *J*-shifting method (WP JS) along with the available QCT data [19]. For both channels of this isotopic variant the WP JS rate constants lie below the QCT rate constants with the exception of very low temperatures. It must be considered that the QCT rates constants were obtained by averaging over the rotational states $j = 0$–4. It has been shown [19] that rotation has a positive effect, increases reactivity, for the NH + D channel and to smaller extent for the ND+H channel in the QCT calculations. On the contrary, the statistical QM method [19] yields excitations functions almost independent of the initial rotational state of HD. Nevertheless, the present WP JS total rate constant (i.e. summing both output channels) at 300 K is 1.73×10^{-12} cm^3 s^{-1} which compares well with the experimental value of 1.83×10^{-12} cm^3 s^{-1} reported by Umemoto et al. [46].

The intramolecular NH/ND isotope effect is represented in the bottom panel of Fig. 11. The WP JS results decrease from 2.5 to 2.2, while the QCT results increases slightly from 2.2 to 2.6 over the temperature range considered. The experimental value of 1.5 at 300 K reported by Umemoto [6] is somewhat lower than the present theoretical estimations.

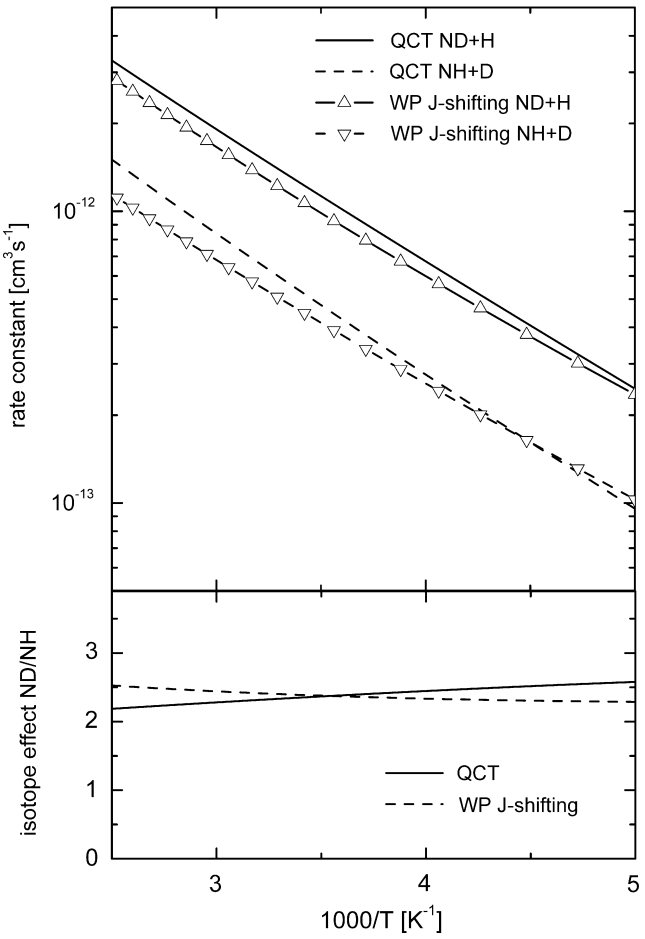

Fig. 11. (Top panel) Rate constants for the two-channel $N(^2D) + HD(v = 0, j = 0)$ reaction. (Bottom panel) Intramolecular ND/NH isotope effect. The lines and lines with symbols correspond to QCT results from Ref. [19] and WP JS results, respectively, as indicated.

4. Conclusions

In this work, we have applied two versions of the quantum time-dependent wave packet methodology, real wave packet and split operator wave packet, and the QCT approach to study the reactive scattering of $N(^2D) + H_2$ system and its isotopic variants. It has been shown that both real wave packet and split operator wave packet methods yield practically the same total reaction probabilities and vibrationally and rotationally state-resolved reaction probabilities for $J = 0$. The corresponding QCT reaction probabilities for $J = 0$ are in reasonable agreement with the present WP results, but underestimate the reactivity near the threshold for each reaction, where tunneling and resonant effects are expected to be more important. Excitation functions for the $N(^2D) + H_2(v = 0, j = 0)$ reaction have been computed using the real wave packet results at $J = 0$ and several *J*-shifting approximations with centrifugal sudden approximation calculations. The agreement found with existing exact time-dependent and time-independent QM results is very satisfactory. For the $N(^2D) + D_2(v = 0, j = 0)$ and $N(^2D) + HD(v = 0, j = 0)$ reactions, the wave packet excitation functions with the simple *J*-shifting approximation are in good accord with the QCT calculations. Rate constants for the $N(^2D) + H_2$ $(v = 0, j = 0)$ reaction have been obtained using the split operator wave packet method in combination with centrifugal sudden approximation calculations and the uniform *J*-shifting method [28]. The agreement found with exact wave packet calculations [21] confirms that the approximate methods are accurate enough to obtain good rate constants for the title reaction. For the $N(^2D) + D_2(v = 0, j = 0)$ reaction, even the simple *J*-shifting scheme yields wave packet rate constants in good agreement with the experimental data and QCT calculations.

Acknowledgements

JFC gratefully acknowledges support from the Spanish Ministry of Education and Science (MEC) through the program "Ramón y Cajal". N.B. thanks a postdoctoral fellowship by Spanish MEC under the Program "Estancias de jóvenes doctores y tecnólogos extranjeros en España". This work has received financial support from the Spanish MEC Grant No. CTQ2005-08493-C02-01 and from the Comunidad de Madrid under the Contrato Programa Comunidad de Madrid-Universidad Complutense de Madrid (Grant No. 910729).

References

[1] J.A. Dodd, S.J. Lipson, D.J. Flanagan, W.A.M. Blumberg, J. Chem. Phys. 94 (1991) 4301.
[2] H. Kobayashi, T. Takayanagi, K. Yokoyama, T. Sato, S. Tsunashima, J. Chem. Soc., Faraday Trans. 91 (1995) 3771.
[3] T. Takayanagi, H. Kobayashi, S. Tsunashima, J. Chem. Soc., Faraday Trans. 92 (1996) 1311.
[4] H. Umemoto, M. Matsumoto, J. Chem. Phys. 104 (1996) 9640.
[5] H. Umemoto, T. Asai, Y. Kimura, J. Chem. Phys. 106 (1997) 4985.
[6] H. Umemoto, Chem. Phys. Lett. 292 (1998) 594.
[7] H. Kobayashi, T. Takayanagi, S. Tsunashima, Chem. Phys. Lett. 277 (1997) 20.
[8] M. Alagia, N. Balucani, L. Cartechini, P. Casavecchia, G.G. Volpi, L.A. Pederson, G.C. Schatz, G. Lendvay, L.B. Harding, T. Hollebeek, T.S. Ho, H. Rabitz, J. Chem. Phys. 110 (1999) 8857.
[9] N. Balucani, M. Alagia, L. Cartechini, P. Casavecchia, G.G. Volpi, L.A. Pederson, G.C. Schatz, J. Phys. Chem. A. 105 (2001) 2414.
[10] A. Pederson, G.C. Schatz, T.S. Ho, T. Hollebeek, H. Rabitz, L.B. Harding, G. Lendvay, J. Chem. Phys. 110 (1999) 9091.
[11] P. Honvault, J.-M. Launay, J. Chem. Phys. 111 (1999) 15.
[12] H. Umemoto, N. Terada, K. Tanaka, J. Chem. Phys. 112 (2000) 5762.
[13] E.J. Rackham, F. Huarte-Larrañaga, D.E. Manolopoulos, Chem. Phys. Lett. 343 (2001) 356.
[14] E.J. Rackham, T. Gonzalez-Lezana, D.E. Manolopoulos, J. Chem. Phys. 119 (2003) 12895.
[15] N. Balucani, L. Cartechini, G. Capozza, E. Segoloni, P. Casavecchia, G.G. Volpi, F.J. Aoiz, L. Bañares, P. Honvault, J.-M. Launay, Phys. Rev. Lett. 89 (2002) 013201.
[16] N. Balucani, P. Casavecchia, L. Bañares, F.J. Aoiz, T. González-Lezana, P. Honvault, J.M. Launay, J. Phys. Chem. A 110 (2006) 817.
[17] T.S. Ho, H. Rabitz, F.J. Aoiz, L. Bañares, S.A. Vázquez, L.B. Harding, J. Chem. Phys. 119 (2003) 6.
[18] T. Suzuki, Y. Shihira, T. Sato, H. Umemoto, S. Tsunashima, J. Chem. Soc., Faraday Trans. 89 (1993) 995.
[19] L. Bañares, F.J. Aoiz, T. González-Lezana, V.J. Herrero, I. Tanarro, J. Chem. Phys. 123 (2005) 224301.
[20] F. Gogtas, N. Bulut, Int. J. Quantum Chem. 106 (2006) 833.
[21] S.Y. Lin, H. Guo, J. Chem. Phys. 124 (2006) 031101.
[22] A.J.C. Varandas, L.A. Poveda, Theor. Chem. Acc. 116 (2006) 4.
[23] T.-S. Chu, K.-L. Han, A.J.C. Varandas, J. Phys. Chem. A 110 (2006) 1666.
[24] A.J.C. Varandas, T.-S. Chu, K.-L. Han, P.J.S.B. Caridade, Chem. Phys. Lett. 421 (2006) 415.
[25] S.K. Gray, G.G. Balint-Kurti, J. Chem. Phys. 108 (1998) 950.
[26] D.E. Manolopoulos, State to State Reaction Dynamics in Encyclopedia of Computational Chemistry, Wiley, Ltd., New York, 1998.
[27] J.M. Bowman, J. Phys. Chem. 95 (1991) 4960.
[28] D.H. Zhang, J.Z.H. Zhang, J. Chem. Phys. 110 (1999) 7622.
[29] V.A. Mandelshtam, H.S. Taylor, J. Chem. Phys. 102 (1995) 7390.
[30] G.J. Kroes, D. Neuhauser, J. Chem. Phys. 105 (1998) 8890.
[31] V.A. Mandelshtam, H.S. Taylor, J. Chem. Phys. 103 (1995) 2903.
[32] A. Vibok, G.G. Balint-Kurti, J. Phys. Chem. 96 (1992) 8712.
[33] G.G. Balint-Kurti, A.I. Gonzalez, E.M. Goldfield, S.K. Gray, Faraday Discuss. 110 (1998) 169.
[34] M. Hankel, G.G. Balint-Kurti, S.K. Gray, Int. J. Quantum Chem. 92 (2003) 205.
[35] F. Gögtas, G.G. Balint-Kurti, C.C. Marston, QCPE Bulletin 14 (1994) 19.
[36] J.Q. Dai, J.Z.H. Zhang, J. Phys. Chem. 100 (1996) 6898.
[37] D.J. Tannor, D.E. Weeks, J. Chem. Phys. 98 (1993) 3884.
[38] R.T. Pack, G.A. Parker, J. Chem. Phys. 87 (1987) 3888.
[39] C.L. Russell, D.E. Manolopoulos, J. Chem. Phys. 110 (1999) 177.
[40] J.C. Light, I.P. Hamilton, V.J. Lill, J. Chem. Phys. 82 (1985) 1400.
[41] M.D. Feit, J.A. Fleck, J. Chem. Phys. 78 (1983) 301.
[42] R.T. Pack, J. Chem. Phys. 60 (1974) 633.
[43] F.J. Aoiz, L. Bañares, V.J. Herrero, J. Chem. Soc., Faraday Trans. 94 (1998) 2483.
[44] L. Bañares, F.J. Aoiz, P. Honvault, J.-M. Launay, J. Phys. Chem. A 108 (2004) 1616.
[45] M.T. Martínez, M.L. Hernández, J.M. Alvariño, F.J. Aoiz, V. Sáez Rábanos, J. Chem. Phys. 119 (2003) 7871.
[46] H. Umemoto, N. Hachiya, E. Matsunag, A. Suda, M. Kawasaki, Chem. Phys. Lett. 296 (1999) 203.